JCS ePress online publication date 20 February 2012

Lysosome fusion to the cell membrane is mediated by the dysferlin C2A domain in coronary arterial endothelial cells

Wei-Qing Han, Min Xia, Ming Xu, Krishna M. Boini, Joseph K. Ritter, Ning-Jun Li and Pin-Lan Li*

Department of Pharmacology & Toxicology, Medical College of Virginia Campus, Virginia Commonwealth University, Richmond, VA 23298, USA

*Author for correspondence (pli@vcu.edu)

Accepted 18 October 2011
Journal of Cell Science 125, 1–10

doi: 10.1242/jcs.094565

Summary

Dysferlin has recently been reported to participate in cell membrane repair in muscle and other cells through lysosome fusion. Given that lysosome fusion is a crucial mechanism that leads to membrane raft clustering, the present study attempted to determine whether dysferlin is involved in this process and its related signalling, and explores the mechanism underlying dysferlin-mediated lysosome fusion in bovine coronary arterial endothelial cells (CAECs). We found that dysferlin is clustered in membrane raft macrodomains after Fas Ligand (FasL) stimulation as detected by confocal microscopy and membrane fraction flotation. Small-interfering RNA targeted to dysferlin prevented membrane raft clustering. Furthermore, the translocation of acid sphingomyelinase (ASMase) to membrane raft clusters, whereby local ASMase activation and ceramide production – an important step that mediates membrane raft clustering – was attenuated. Functionally, silencing of the dysferlin gene reversed FasL-induced impairment of endothelium-dependent vasodilation in isolated small coronary arteries. By monitoring fluorescence quenching or dequenching, silencing of the dysferlin gene was found to almost completely block lysosome fusion to plasma membrane upon FasL stimulation. Further studies to block C2A binding and silencing of *AHNAK* (a dysferlin C2A domain binding partner), showed that the dysferlin C2A domain is required for FasL-induced lysosome fusion to the cell membrane, ASMase translocation and membrane raft clustering. We conclude that dysferlin determines lysosome fusion to the plasma membrane through its C2A domain and it is therefore implicated in membrane-raft-mediated signaling and regulation of endothelial function in coronary circulation.

Key words: Ferlin, Vesicle fusion, Molecular trafficking, Arterial endothelium

Introduction

Dysferlin is a 230 kDa membrane-spanning protein with multiple C2 domains that bind calcium, phospholipids and proteins to trigger signaling events, vesicle trafficking and membrane fusion (Davis et al., 2002; Cenacchi et al., 2005; Han et al., 2007; Evesson et al., 2010). Studies have shown that dysferlin is involved in muscle membrane repair by mediating vesicle fusion with the plasma membrane, and that lysosomes might be one of the intracellular vesicles that participate in the process. Further studies have shown that in sarcolemmal wound healing, lysosome-associated membrane protein (Lamp-1) decreases in the sarcolemma of myocytes from dysferlin-knockout mice, indicating that dysferlin gene expression is important for lysosome-associated wound healing. This wound-healing process is dependent on Ca^{2+} influx because removal of Ca^{2+} from the extracellular medium decreased sarcolemmal expression of Lamp-1, which might be due to reduction of lysosome fusion to the sarcolemma of the muscle cells. In electron micrographs of dysferlin-null myoblasts, enlarged dense-core granules were seen to accumulate near the plasma membrane, whereas confocal microscopy showed the accumulation of enlarged Lamp-2-positive vesicles near the nucleus and in the cell extensions, but not to the same extent as observed in wild-type cells, pointing toward a trafficking defect in lysosomes of dysferlin-null cells (Demonbreun et al., 2011).

Of the seven predicted C2 domains, the dysferlin C2A domain binds to phosphatidylserine and phosphoinositides in a Ca^{2+}-dependent fashion, whereas the others show weaker and calcium-independent binding to phosphatidylserine and no binding to phosphoinositides (Therrien et al., 2009). Importantly, a point mutation in the dysferlin C2A domain, V67D, which is responsible for limb-girdle muscular dystrophy type 2B and distal myopathy (Illarioshkin et al., 2000), abolishes calcium-induced C2A binding to phospholipids in vitro (Illarioshkin et al., 2000; Davis et al., 2002). In addition to binding of lipids, the C2A domain also binds various protein partners needed for dysferlin-mediated membrane fusion. For example, dysferlin has been shown to bind annexin A1 and annexin A2 following membrane injury, and the distribution of these annexins after injury is significantly altered in dysferlin-deficient skeletal muscle (Lennon et al., 2003). Furthermore, inhibition of its function using an annexin A1 function-blocking antibody, a small peptide competitor of annexin A1 or a dominant-negative annexin A1 mutant protein incapable of Ca^{2+} binding, prevents lysosome fusion and membrane resealing (McNeil et al., 2006). AHNAK is an exceptionally large protein (~600–700 kDa) that is uniformly distributed on the plasma membrane of normal skeletal muscle. Structural analysis does not provide any evidence for the presence of transmembrane domains in AHNAK (Chai et al.,

Journal of Cell Science

2006). A recent study has shown that the C-terminal domain of AHNAK interacts with the dysferlin C2A domain. In regenerating rat muscle, there is a marked increase of both dysferlin and AHNAK, but in contrast to dystrophin, which remains preferentially associated with the plasma membrane, AHNAK shows a marked shift to a cytoplasmic localization in regenerating rat muscle, indicating that AHNAK has a role in the dysferlin-mediated membrane repair process (Chai et al., 2006). However, there is no evidence that this dysferlin-mediated lysosome fusion and consequent cell membrane repair occur in vascular endothelial cells.

Our previous studies showed that lysosome trafficking to the plasma membrane and fusion to plasma membrane are crucial mechanisms initiating membrane raft clustering upon Fas ligand (FasL) stimulation of CAECs (Shao et al., 2003; Jin et al., 2008a; Bao et al., 2010). Through lysosome fusion, lysosomal ASMase is translocated into the membrane, where it is then activated (Shao et al., 2003; Jin et al., 2008a; Bao et al., 2010). The product of ASMase (ceramide) then triggers clustering of membrane rafts to form membrane rafts macrodomains or platforms (Jin et al., 2007; Zhang, A. Y. et al., 2007). Importantly, the subunits of NADPH (nicotinamide adenine dinucleotide phosphate) oxidase including $gp91^{phox}$ and $p22^{phox}$ are also aggregated in these complexes upon stimulation by death factors such as FasL, tumor necrosis factor alpha (TNF-α) and endostatin, leading to its activation, which produces superoxide ($O_2\cdot^-$) and consequent endothelial dysfunction (Zhang, A. Y. et al., 2006).

Of note, it has been reported that dysferlin is localized in membrane raft fractions of human endothelial cells (Karsan et al., 2005). We therefore hypothesized that dysferlin is involved in FasL-induced lysosome fusion with the plasma membrane by a mechanism involving its C2A domain in CAECs, which mediates membrane raft clustering and activation of NADPH oxidase, leading to endothelial dysfunction.

Results

Involvement of dysferlin in FasL-induced membrane raft clustering and aggregation of ASMase and dysferlin in CAECs

Fig. 1A presents representative fluorescent microscopic images for membrane raft clusters as shown by patches labeled with Alexa-Fluor-488-conjugated cholera toxin B (Alexa488–CTXB) on the cell membrane. Under resting conditions, membrane rafts were distributed across the cell membrane, indicated by the weak, diffuse green fluorescence. Upon stimulation with FasL, clustering of membrane rafts occurred, as indicated by the appearance of brighter patches of green fluorescence. In the data summary shown in Fig. 1B, only a small percentage of the resting cells exhibited these clusters (17%), whereas the percentage increased almost fourfold after FasL treatment (Fig. 1B). This clustering of membrane rafts was blocked by prior transfection of the cells with siRNA to knock down dysferlin (*DYSF* siRNA). Co-staining of the Alexa488–CTXB-labeled cells revealed that dysferlin and ASMase were aggregated in these clusters (Fig. 1A,B) after FasL stimulation, and the aggregation of both was completely prevented by silencing of the gene encoding dysferlin (Fig. 1C).

Furthermore, FasL-induced changes in the membrane distribution of dysferlin were evaluated by using a detergent-resistant membrane fraction flotation assay. As shown in Fig. 1D, the expression of flotillin-1, a membrane-raft-specific marker,

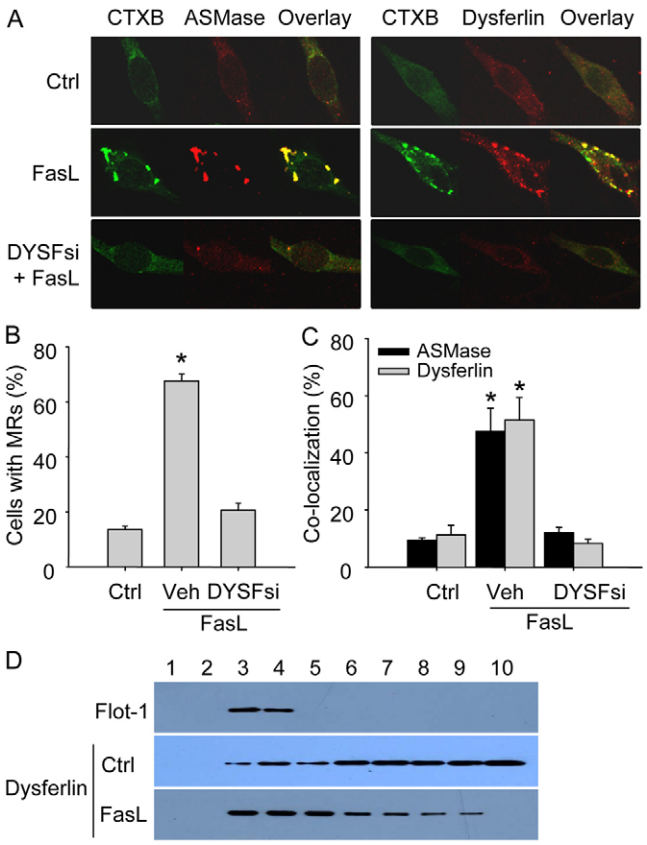

Fig. 1. Effect of dysferlin knockdown on FasL-induced membrane raft clustering in CAECs. (**A**) Representative confocal microscopic images showing inhibition by dysferlin siRNA of FasL-induced formation of membrane raft clusters, colocalization of membrane raft clusters with ASMase (left) and dysferlin (right) in 5–6 batches of cells. (**B**) Summarized data showing the effects of dysferlin siRNA on the numbers of membrane raft clusters in response to FasL stimulation. MR, membrane raft. (**C**) Summarized data showing the effects of dysferlin siRNA on FasL-induced colocalization of membrane raft clusters with ASMase and dysferlin. *$P<0.05$ vs other groups. (**D**) CAECs treated with or without stimulation of FasL for 20 minutes were subjected to immunoblot analysis of either flotillin-1 or dysferlin. Numbers (1–10) on the top indicate membrane fractions isolated by gradient centrifugation from the top to bottom. Fractions 1–2 were very light fractions without proteins. Fractions 3–5 were light fractions designated as membrane rafts based on the presence of the LR marker protein, flotillin-1 (flot-1). The heavier fractions 6–10 were designated as non-raft fractions and contained membrane and cytosolic proteins.

was primarily found in the fractions (2–4) between the 5% and 30% gradients. In control cells, dysferlin was mainly found in the non-lipid-raft domain, and FasL treatment caused a marked shift in dysferlin distribution from a non-lipid-raft domain to membrane raft domain (Fig. 1D).

Dysferlin inhibition blocks FasL-induced ASMase activation and ceramide production

Because our previous studies have shown that translocation of ASMase results in its activation and increased ceramide production in situ, we evaluated whether silencing of dysferlin gene expression would prevent these changes. Fig. 2A shows that in CAECs transfected with scrambled RNA, FasL treatment markedly increased the ASMase activity as detected using the

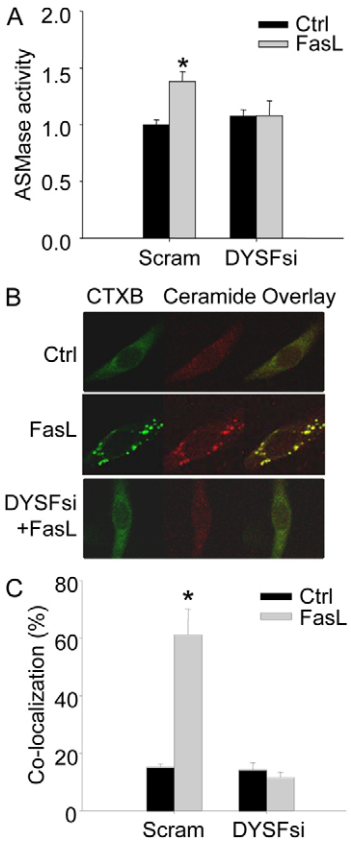

Fig. 2. Inhibitory effect of *DYSF* siRNA on FasL-induced ASMase activation in CAECs. (**A**) CAECs treated with either control (scrambled) sRNA or dysferlin siRNA were stimulated with 10 ng/ml FasL for 15 minutes and then prepared for ASMase activity. $n=5$ batches of cells; $^*P<0.05$ vs scrambled siRNA group. Representative confocal microscopic images (**B**) and summarized data (**C**) showing the effect of dysferlin siRNA on colocalization of membrane rafts and ceramide in CAECs. $n=5$–6 batches of cells; $^*P<0.05$ vs scrambled siRNA group.

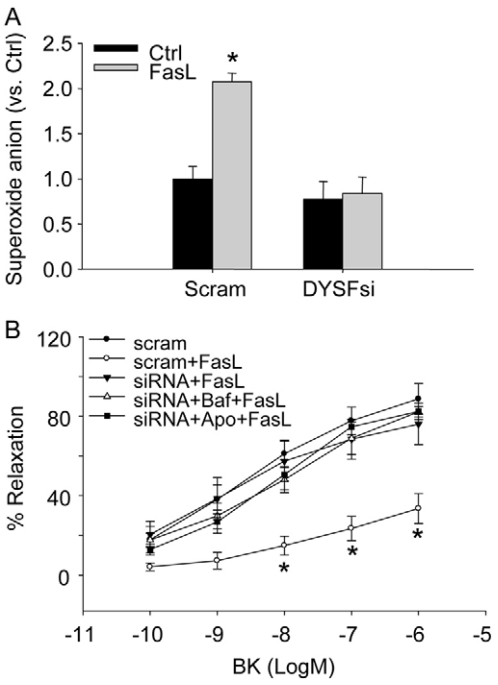

Fig. 3. Dysferlin gene silencing blocks FasL-induced ROS production and reverses FasL-induced inhibition of the endothelium-dependent vasodilator response to bradykinin. (**A**) Inhibitory effect of *DYSF* siRNA on $O_2\cdot^-$ production in CAECs measured using ESR spectrometry. $n=5$–6 batches of cells; $^*P<0.05$ vs scram group. (**B**) Reversal by *DYSF* siRNA of FasL-impaired vasodilator responses to increasing bradykinin doses in small, isolated bovine coronary arteries. The combination of FasL and *DYSF* siRNA with either the lysosome function inhibitor, Baf, or the NADPH oxidase inhibitor, apocynin, had no additional effect compared with dysferlin siRNA + FasL stimulation group. $n=5$ cow hearts. $^*P<0.05$ vs scrambled sRNA, dysferlin siRNA + FasL, dysferlin siRNA + Baf + FasL, or dysferlin siRNA + apocynin + FasL group.

^{14}C-choline phosphate assay. In the CAECs transfected with *DYSF* siRNA, however, the FasL-induced increase in ASMase activity was significantly attenuated. We also measured local ceramide production in single CAECs by staining with antibody against ceramide. As shown in Fig. 2B, ceramide production was localized with membrane raft clusters (yellow patches) in the cell membrane, which was markedly increased in FasL-stimulated CAECs. In the CAECs with dysferlin knockdown, the FasL-induced increase in ceramide production in membrane raft clusters was almost completely blocked (Fig. 2B). These results are summarized in Fig. 2C.

Dysferlin knockdown inhibits FasL-induced $O_2\cdot^-$ production and reverses FasL-induced impairment of endothelium-dependent vasodilation

In previous studies, the activation of death receptors by FasL and other ligands was shown to lead to increased production of $O_2\cdot^-$ by endothelial cells as a result of the assembly and activation of an NADPH oxidase in membrane raft signaling platforms. To assess the role of dysferlin in this cellular response, CAECs were transfected with either scrambled or dysferlin siRNA, and the production of $O_2\cdot^-$ in the absence and presence of FasL was measured by electron spin resonance (ESR). FasL stimulated $O_2\cdot^-$ production in scrambled siRNA-transfected CAECs, but not in the cells transfected with *DYSF* siRNA (Fig. 3A).

The involvement of dysferlin in FasL-induced endothelial dysfunction was determined using isolated coronary artery segments. Fig. 3B shows that addition of bradykinin produced a concentration-dependent relaxation in these small coronary arteries, but in the presence of FasL, bradykinin-induced vasodilation was significantly attenuated. Prior transfection of endothelial cells in the isolated coronary arteries with *DYSF* siRNA prevented the FasL-induced impairment of vasodilation. Notably, treatment with either bafilomycin A (Baf), a lysosome function inhibitor, or apocynin, an NADPH oxidase inhibitor, had no further effect on the inhibition mediated by knockdown of dysferlin. Both Baf and apocynin were shown previously to prevent the FasL-induced impairment of bradykinin vasodilation (Zhang, A. Y. et al., 2006; Jin et al., 2008b). These findings indicate that *DYSF* siRNA reverses FasL-induced impairment of vasodilation, at least in part, through the inhibition of lysosome fusion and NADPH oxidase-derived $O_2\cdot^-$.

Involvement of dysferlin in FasL-induced lysosomal fusion

Because previous studies showed that lysosome fusion triggers lysosomal ASMase translocation and membrane raft clustering,

we next examined the role of dysferlin in FasL-induced lysosome fusion using the lysosomal dye (FM1-43) quenching assay. For this experiment, CAECs were incubated with FM1-43 for 2 hours to preload the lysosomes, then bromide Phenol Blue (BPB) was added, followed immediately by treatment with FasL. Lysosome fusion was detected by a decrease in FM1-43 fluorescence that occurred after FasL treatment, which is due to release of the dye into the external medium followed by its quenching with BPB, a membrane-impermeant quencher. Therefore, FM1-43 fluorescence quenching indicates lysosome fusion. Under control (unstimulated) conditions, FM1-43-loaded CAECs exhibited sustained fluorescence over a 30 minute time period (data not shown). When the cells were stimulated with FasL, a marked reduction of fluorescence intensity occurred over the same time period as shown by confocal fluorescence images and continuous recording of changes in fluorescence intensity in lysosomes of CAECs (Fig. 4A). In such recordings, each curve represents fluorescence change from one lysosome of the ECs. When these cells were transfected with *DYSF* siRNA, FasL-induced quenching was significantly inhibited, and this inhibitory effect

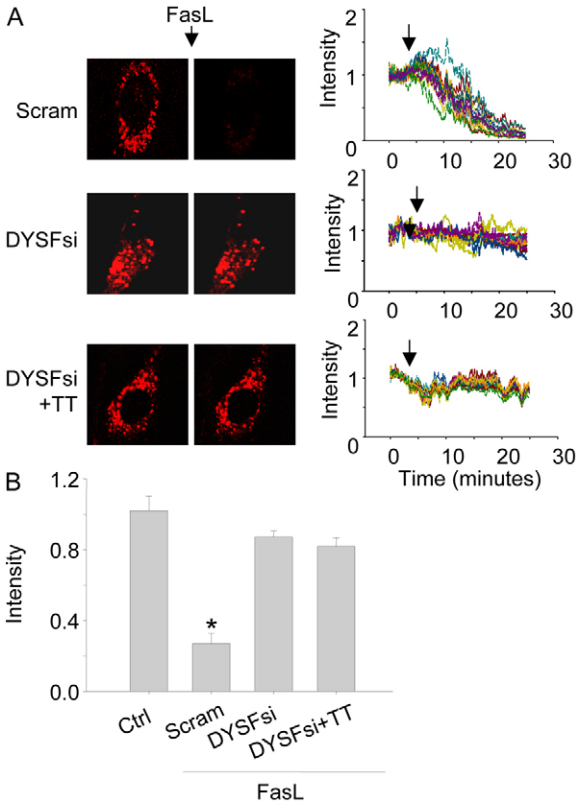

Fig. 4. *DYSF* siRNA blocks FasL-induced lysosomal fusion and exocytosis in CAECs. (**A**) Representative confocal microscopic images (left) and fluorescence traces (right) showing the inhibition by *DYSF* siRNA of FasL-induced quenching of FM1-43 fluorescence in bovine CAECs. Cells were pre-loaded with FM1-43, and BPB was added immediately before FasL treatment. The arrows indicate the beginning of the FasL treatment. (**B**) Changes in FM1-43 fluorescence in CAECs treated with control siRNA, *DYSF* siRNA, and *DYSF* siRNA in combination with the VAMP-2 inhibitor tetanus toxin (TT). For each group, the change in fluorescence was normalized to the fluorescence intensity obtained immediately prior to FasL treatment. $n=6$ batches of cells; $^{*}P<0.05$ vs other groups.

was not further increased by addition of the vesicle-associated membrane protein 2 (VAMP-2) inhibitor tetanus toxin (TT). These results are summarized in Fig. 4B. It is clear that FasL-induced maximal changes in F-l43 quenching were substantially blocked by knockdown of dysferlin and TT had no further inhibitory effect, indicating that the normal expression and function of dysferlin is crucial for lysosome fusion upon FasL stimulation, and that dysferlin might be involved in the same signaling pathway as VAMP-2 in the regulation of lysosome fusion.

Inhibitory effect of phosphatidylserine and phosphatidylinositol 4-phosphate on FasL-induced lysosome fusion and the downstream signaling pathway

To evaluate whether dysferlin mediates lysosome fusion through its C2A domain, which binds lipid such as phosphatidylserine or phosphatidylinositol 4-phosphate (PIP), the effect of adding excess phosphatidylserine to the incubation solution was tested. As shown in Fig. 5, treatment with phosphatidylserine inhibited or completely blocked the FasL-induced clustering of membrane rafts and the aggregation of either ASMase or dysferlin in the membrane raft clusters. Under such conditions, the FasL-induced increase in ASMase activity was completely blocked by addition of excess phosphatidylserine (Fig. 6), whereas lysosome fusion detected using the FM1-43 quench assay was greatly inhibited (Fig. 7). The effect of a second lipid that also binds strongly to the C2A domain of dysferlin, PIP, was also evaluated. PIP treatment resulted in almost identical effects on membrane raft clustering, translocation of ASMase and aggregation of dysferlin in the clustered membrane rafts (Fig. 5), activation of ASMase (Fig. 6) and lysosome fusion (Fig. 7). These results indicate that excessive phosphatidylserine and PIP might saturate the functional C2A domain and render it unable to react with lysosomes, thereby blocking FasL-induced lysosome fusion and consequent membrane raft clustering.

AHNAK RNAi attenuates FasL-induced lysosome fusion and the downstream signaling pathway

We also evaluated whether the AHNAK protein is involved in dysferlin-mediated lysosome fusion, given that AHNAK serves as a dysferlin binding partner and thereby plays a critical role in dysferlin-mediated membrane repair (Chai et al., 2006). We found that treatment with siRNA to knock down AHNAK inhibited FasL-induced membrane raft clustering, ASMase translocation and activation, and lysosome fusion was also significantly decreased (Figs 5–7). These results indicate that AHNAK is involved in dysferlin-mediated lysosome fusion in CAECs.

Dysferlin C2A domain lipid-binding peptide inhibits FasL-induced lysosome fusion

To confirm the involvement of the dysferlin C2A domain, a 20-residue peptide was synthesized according to the sequence of the conserved dysferlin C2A domain, and the lipid binding capacity and its effect on lysosome fusion were evaluated. The lipid binding capacity was evaluated by comparing the peptide concentrations before and after the binding reaction. If the concentration decreases after binding reaction, it indicates that the peptide is bound with lipid and trapped in spin columns. As shown in Fig. 8A, wild-type DYSF C2A peptide (C2A-V) showed a high lipid binding capacity. When the Val residue of

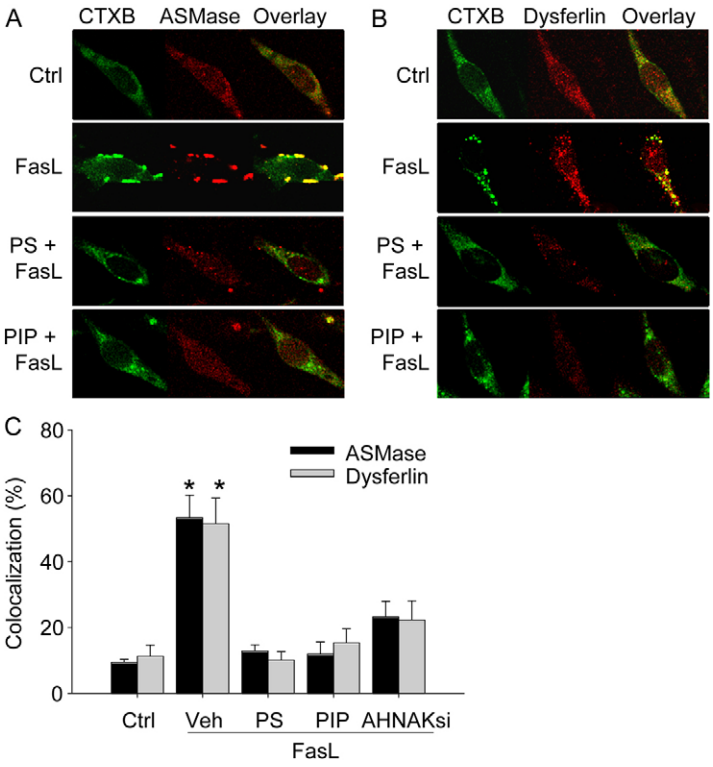

Fig. 5. Excess phosphatidylserine and PIP, and siRNA against AHNAK inhibit FasL-induced formation of membrane raft clusters and colocalization of membrane raft clusters with ASMase and dysferlin. Representative confocal microscopic images (**A**,**B**) and summarized data (**C**) showing the inhibitory effect of phosphatidylserine and PIP, and siRNA against AHNAK on colocalization between membrane raft clusters and ASMase, dysferlin. n=5~6 batches of cells. *P<0.05 vs other groups for each treatment.

this peptide sequence was replaced with an Asp (C2A-D), the lipid binding ability was significantly inhibited. By contrast, the dysferlin C2F domain peptide showed a very low lipid binding capacity. Using these peptides, we performed functional studies to observe their effects on lysosome fusion. Wild-type DYSF C2A peptide effectively inhibited FasL-induced lysosome fusion as shown by FM1-43 quenching, whereas mutant DYSF C2A and DYSF C2F peptides had no inhibitory effect (Fig. 8B,C). Such effects were due to the binding capacity of wild-type DYSF C2A peptide, which diverted the lipids of lysosomes by blocking their binding to normal dysferlin on the cell membrane. These data further support the view that the dysferlin C2A domain plays a critical role in FasL-induced lysosome fusion.

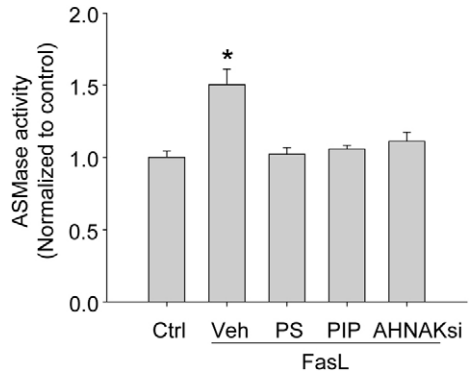

Fig. 6. Excess phosphatidylserine and PIP, and siRNA against AHNAK inhibit FasL-induced ASMase activation in CAECs. ASMase activity was measured by quantification of production of choline phosphate using radiometry. n=6 batches of cells; *P<0.05 vs other groups.

Discussion

The present study characterized the expression of dysferlin in CAECs and found that this ferlin protein becomes aggregated in membrane raft clusters upon stimulation with FasL. Using siRNA-mediated gene silencing, we showed that dysferlin expression in CAECs is necessary for FasL-induced membrane raft clustering, which drives translocation of ASMase into membrane raft clusters, activates ASMase, causes ceramide enrichment of membrane raft clusters and leads to the formation of a functional membrane raft to NADPH oxidase signaling platform. Functionally, dysferlin is required for the inhibitory effects of FasL on the endothelium-dependent vasodilation. The data support a direct role for lysosome fusion mediated by dysferlin as a crucial mechanism of FasL-induced endothelial dysfunction, acting through the C2A domain of dysferlin.

The finding that dysferlin protein was abundantly expressed in bovine CAECs (supplementary material Fig. S1) is consistent with other studies describing the presence of dysferlin in endothelial cells (Karsan et al., 2005; Hochmeister et al., 2006). Subcellular localization assays showed that dysferlin is mainly detected in the cell homogenate rather than the microsomal or cytosol fractions (Matsuda et al., 1999), and it was located on plasma membrane and intracellular vesicles in permeabilized CAECs (supplementary material Fig. S1). These results indicate that dysferlin is a membrane-associated protein, which is located on the plasma membrane and intracellular vesicles. In agreement with a previous study that dysferlin was aggregated at sites of membrane injury, the present study showed by confocal microscopy that dysferlin is clustered in membrane rafts in CAECs upon stimulation with FasL, indicating that dysferlin might be involved in membrane raft clustering. Such membrane raft association of dysferlin was further supported by

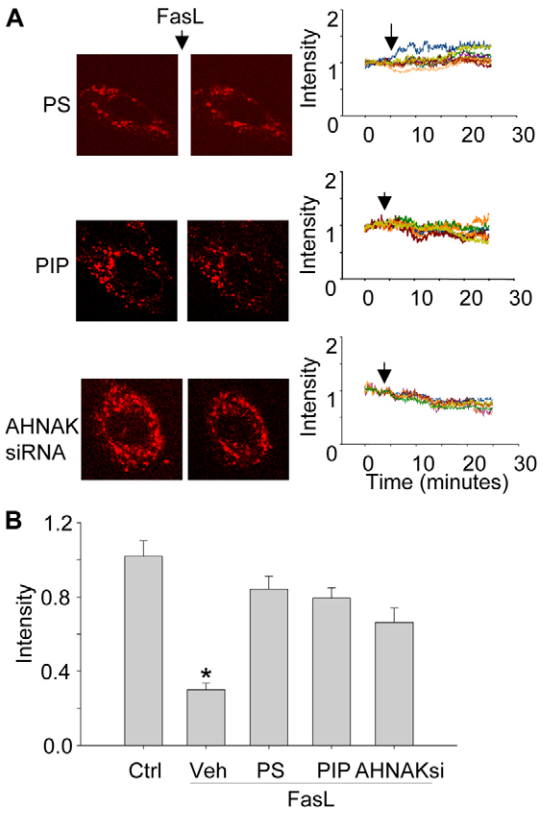

Fig. 7. Excess phosphatidylserine and PIP, and siRNA against AHNAK inhibit FasL-induced lysosome fusion in CAECs. (**A**) Representative confocal microscopic images (left) and fluorescence traces (right) showing the inhibition of FasL-induced FM1-43 quenching by phosphatidylserine, PIP and siRNA against AHNAK in bovine CAECs. Cells were pre-loaded with FM1-43, and BPB was added immediately before FasL treatment. The arrows show the beginning of FasL treatment. (**B**) Summarized data showing the changes in FM1-43 fluorescence after FasL treatment in CAECs with or without phosphatidylserine PIP, and siRNA against AHNAK. For each group, the change in fluorescence was normalized to the fluorescence intensity obtained immediately before FasL treatment. $n=5-6$ batches of cells, $^*P<0.05$ vs other groups.

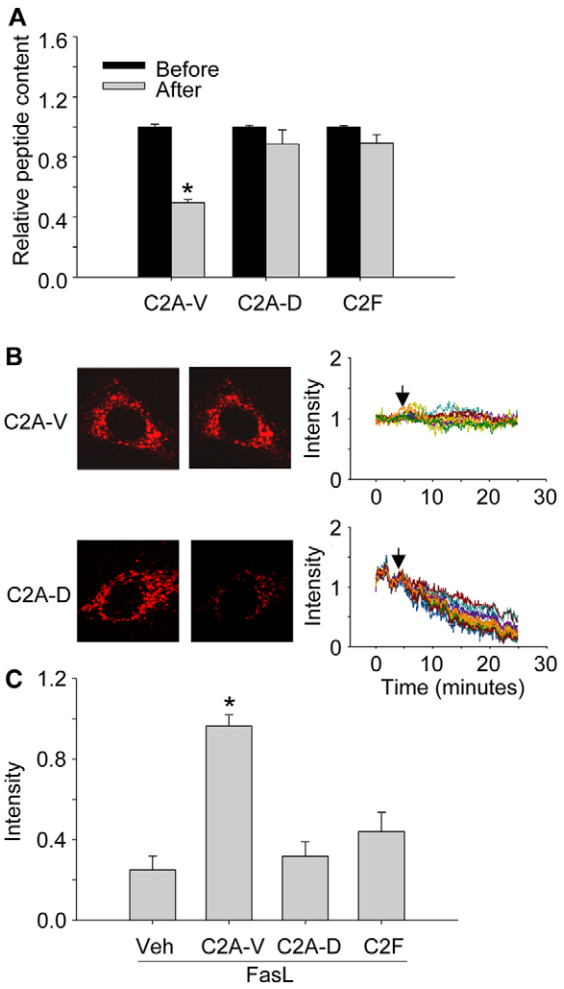

Fig. 8. Dysferlin C2A domain peptide inhibits FasL-induced lysosome fusion. (**A**) Lipid binding capacity of wild-type dysferlin C2A peptide, mutated dysferlin C2A peptide, and dysferlin C2F peptide. (**B**) Representative confocal microscopic images (left) and fluorescence traces (right) showing the effect of wild-type dysferlin C2A peptide, mutated dysferlin C2A peptide on FasL-induced FM1-43 quenching in bovine CAECs. Cells were pre-loaded with FM1-43, and BPB was added immediately before FasL treatment. The arrows show the beginning of FasL treatment. (**C**) Summarized data showing the changes in FM1-43 fluorescence in CAECs after FasL treatment with or without the wild-type dysferlin C2A peptide, mutated dysferlin C2A peptide, and dysferlin C2F peptide. For each group, the change in fluorescence was normalized to the fluorescence intensity obtained immediately before FasL treatment. C2A-V, wild-type dysferlin C2A peptide; C2A-D, mutated dysferlin C2A peptide; C2F, dysferlin C2F peptide. $n=4\sim6$ batches of cells. $^*P<0.05$ vs other groups for each treatment.

the observed FasL-stimulated shift of dysferlin from the non-raft to membrane raft domains in the membrane fraction flotation assay, which is consistent with a previous study reporting that dysferlin exists in the detergent-resistant fraction of endothelial cell membranes (Karsan et al., 2005). These results together provide convincing evidence on the association of dysferlin with membrane rafts and their clustering in CAECs.

To test the contribution of dysferlin to lysosome fusion and related signaling events associated with membrane raft clustering, the RNA interference strategy was used given that there are no specific inhibitors or blockers of dysferlin reported so far. The effectiveness of dysferlin-specific siRNA was confirmed by real-time PCR and western blot analysis, which showed a large decrease in the relative level of dysferlin protein in CAECs treated with *DYSF* siRNA (supplementary material Fig. S2). The siRNA-mediated decrease in dysferlin expression produced a significant attenuation of FasL-induced membrane raft clustering, indicating that dysferlin is directly involved in this process. To further determine the role of dysferlin in signaling events downstream of membrane raft clustering, we examined the effects of *DYSF* siRNA on ASMase translocation, ceramide production and the formation and function of the redox signaling platform. It has been well documented that FasL causes the translocation of ASMase to the plasma membrane followed by its activation. The product of ASMase, ceramide, then drives the formation of large ceramide-enriched platforms, with clustering or aggregation of different signaling molecules such as NADPH oxidase subunits, which are assembled and activated to produce redox signaling. This series of signaling events constitutes a membrane signalosome, which is a multiple protein reaction complex (Gulbins and Li, 2006; Touyz, 2006; Zhang, A. Y. et al.,

2006; Zhang, A. Y. et al., 2007; Jin et al., 2008b). In vascular endothelial cells, NADPH oxidase subunits are aggregated and assembled in clustered membrane raft domains in response to FasL stimulation, leading to the activation of this enzyme to form redox signalosomes (Jin et al., 2008b; Jin et al., 2008a; Eum et al., 2009). In agreement with the disruption of membrane raft clustering, *DYSF* siRNA was found to prevent FasL-induced translocation of ASMase to membrane raft clusters and its activation (supplementary material Fig. S3), and local ceramide production and membrane raft clustering induced by FasL were significantly blocked. The florescence intensity of ASMase and dysferlin on the plasma membrane in intact endothelial cells increased significantly in response to FasL treatment, whereas total ASMase, dysferlin and GM1 were not changed in dot blot and immunoblot analysis (supplementary material Fig. S4). These results indicated that ASMase and dysferlin are translocated to plasma membrane in response to FasL treatment, and then are involved in lipid raft clustering. Moreover, NADPH oxidase subunit aggregation and its activation were also suppressed by treatment with *DYSF* siRNA, as demonstrated by the results from the ESR spectrometry, where NADPH oxidase activity was inhibited by *DYSF* siRNA pretreatment. Correspondingly, vascular reactivity measurements showed that treatment with *DYSF* siRNA reversed FasL-induced impairment of the vasodilatory curves to bradykinin. In our previous study, lysosome function was found to play a crucial role in mediating superoxide production and related impairment of endothelium-dependent vasodilation upon FasL stimulation, which occurred through its contribution to membrane raft clustering. This lysosome-mediated action could be blocked by Baf, methyl-b-cyclodextrin and apocynin (Zhang, A. Y. et al., 2006; Li, P. L. et al., 2007). In the present study, we used these inhibitors together with *DYSF* siRNA and found that there are no additive effects observed. It seems that when dysferlin expression is blocked, superoxide production decreases through apocynin-sensitive NADPH oxidase activity and lysosome-related membrane raft clustering.

In previous studies, dysferlin was shown to be crucial for plasma membrane repair in skeletal muscle cells by a mechanism involving the fusion of intracellular vesicles, probably lysosomes, with the plasma membrane in response to membrane disruption (Reddy et al., 2001). In CAECs, FasL-induced membrane raft clustering and formation of the redox signaling platform were demonstrated to be associated with lysosome fusion (Zhang, Z. et al., 2007; Jin et al., 2008b). Therefore, we next tested whether the role of dysferlin in mediating membrane raft clustering is due to its action mediating lysosome fusion to cell membrane, translocating ASMase to produce ceramide and promoting membrane raft clustering. To test this hypothesis, the FM1-43 quenching assay was used to determine FasL-induced lysosome fusion in CAECs. It was found that *DYSF* siRNA almost fully abolished FasL-induced lysosome fusion, indicating that dysferlin might directly mediate FasL-induced lysosome fusion, which is consistent with previous studies showing dysferlin-mediated lysosome fusion with plasma-membrane-mediated muscle and myoblast membrane healing (Lennon et al., 2003; Han et al., 2007). Dysferlin has been shown by the recruitment of intracellular membrane components to repair the plasma membrane in animal models, human diseases and in cells treated with various stimuli such as lasers, irradiation or mechanical stress (Matsuda et al., 1999; Han et al., 2007; Lek et al., 2011). The present study demonstrated that dysferlin is also involved in the endothelial membrane rafts and redox signaling pathway, therefore it might play a role in the regulation of endothelial function and contribute to the development of vascular diseases such as atherosclerosis, hypertension or peripheral arterial disease.

To further explore the mechanism by which dysferlin mediates lysosome fusion in CAECs, we examined the role of the C2 domain of this ferlin protein in such cellular activity. Of the seven C2 domains present in dysferlin, the C2A domain interacts with negatively charged phospholipids, such as phosphoinositides and phosphatidylserine, and proteins such as AHNAK, annexin A1, annexin A2 and tubulin, as well as Ca^{2+}, and therefore this C2 domain might be crucial for dysferlin-mediated vesicle fusion (Azakir et al., 2010; Lennon et al., 2003; Chai et al., 2006; Therrien et al., 2009). In previous studies, exogenously supplied phosphatidylserine and PIP are incorporated and translocated to the inner leaflet of the plasma membrane, and then transported to intracellular organelles such as the Golgi and mitochondria (Kobayashi and Arakawa, 1991; Uchida et al., 1998). Importantly, the dysferlin C2A domain exhibits high-affinity binding to phosphatidylserine and PIP that is regulated by intracellular Ca^{2+} concentrations (Therrien et al., 2009). It is proposed that the influx of Ca^{2+} activates the C2A domain of dysferlin (Doherty and McNally, 2003; Lennon et al., 2003; Han et al., 2007), which promotes the interaction of plasma membrane dysferlin with vesicular phosphatidylserine and phosphoinositides, and of vesicular dysferlin with plasma membrane phosphatidylserine and phosphoinositides, resulting in their fusion. In addition to these events, intervesicular interactions between dysferlin and phosphatidylserine or phosphoinositides generate membrane patches with enriched dysferlin, which are needed to reseal the membrane tears (Doherty and McNally, 2003; Lennon et al., 2003; Han et al., 2007; Therrien et al., 2009). In the present study, excessive phosphatidylserine and PIP added to the culture medium effectively attenuated dysferlin-mediated lysosome fusion. These results support the view that the dysferlin C2A domain is crucial for the function of dysferlin in mediating lysosome fusion and that high dosage of phosphatidylserine and PIP might bind the dysferlin C2A domain and thereby interfere with its interaction with lipids or proteins on the cell membrane or intracellular vesicles. To more specifically identify the involvement of the dysferlin C2A domain, specific peptides corresponding to the lipid binding domains were designed as reported previously (Bommert et al., 1993; Therrien et al., 2009). It was found that the dysferlin C2A domain, but not C2F domain had a high lipid-binding capacity and effectively inhibited FasL-induced lysosome fusion. By contrast, a peptide with a Val–Asp mutation showed no lipid-binding capacity and failed to affect FasL-induced lysosome fusion. These results further support the view that the dysferlin C2A domain is important in mediating lysosome fusion in endothelial cells.

Another novel finding in the present study is that inhibition of AHNAK using an siRNA-mediated gene-silencing strategy effectively attenuated FasL-induced lysosome fusion, as observed by the FM1-43 quenching assay. The deduced amino acid sequence of human AHNAK predicts a protein of 5643 amino acids, which can be divided into three main structural regions: the N-terminal 251 amino acids, a large central region of 4390 amino acids composed of a 128-residue unit repeated 26 times, and the C-terminal 1002 amino acids (Chai et al., 2006). This protein has

been reported to be a partner of dysferlin during its binding to lipids for repair of cell membrane (Chai et al., 2006). Our findings that knockdown of AHNAK attenuated FasL-induced lysosome fusion and the downstream signaling pathway indicates that AHNAK is a binding partner of dysferlin in the formation of a functional dysferlin complex that is necessary for proper vesicle trafficking or fusion, in particular, for lysosome fusion to the cell membrane to promote membrane raft clustering in CAECs.

In summary, the present study demonstrates that dysferlin mediates lysosome fusion to the plasma membrane and thereby leads to ASMase translocation, membrane raft clustering and NADPH oxidase activation in CAECs, which consequently results in endothelial dysfunction. This novel transmembrane signaling mechanism in coronary endothelial cells might contribute to the regulation of endothelial function under different physiological and pathological conditions.

Materials and Methods

Cell culture and stimulation

Bovine CAECs were isolated and maintained in RPMI 1640 (Invitrogen, Carlsbad, CA) containing 10% fetal bovine serum (FBS, HyClone, Waltham, MA) and 1% antibiotics (Sigma, St Louis, MO) as described previously (Jin et al., 2008b). All cell studies were performed by using CAECs of 2 to 4 passages. According to some preliminary experiments and previous studies, the period of 15 minutes was applied for FasL stimulation (10 ng/ml) to induce lysosome fusion and membrane raft clustering and to avoid other actions such as apoptosis (Bao et al., 2010). To test the contribution of dysferlin to lysosome fusion and membrane raft clustering, CAECs were pretreated with different siRNAs or inhibitors as described in individual experiments below. In some groups of CAECs, the binding capacity of the dysferlin C2A domain was saturated by treatment of these cells with 100 μM phosphatidylserine or 4 μM PIP for 30 minutes at 37℃, which blocked its further binding to lipid on vesicles, interfering with dysferlin function.

Immunohistochemistry and immunocytochemistry

Immunohistochemical and immunocytochemical analyses were performed as described previously (Li, N. et al., 2007). In brief, after bovine arteries or bovine CAECs were washed with phosphate-buffered saline (PBS) three times, the samples were fixed with 4% paraformaldehyde. Tissues were embedded in paraffin and were cut in transverse sections (5 μm thick). After they were defatted and rehydrated, slides were probed with antibody against dysferlin (Novus Biologicals, Littleton, CO) and secondary antibody, and then horseradish peroxidase-conjugated streptavindin (streptavindin-HRP) was added.

Colocalization studies

CAECs were fixed with 4% paraformaldehyde in PBS for 10 minutes. After permeabilization with 0.5% Tween-20 for 15 minutes, cells were incubated with rabbit anti-dysferlin antibody (1:50) and Alex-Fluor-488-conjugated goat anti-rabbit antibody (1:500, Molecular Probes, Carlsbad, CA). After washing with PBS, CAECs were incubated with mouse anti-caveolin-1 antibody (1:500, Abcam, San Francisco, CA) or mouse anti-Lamp-1 antibody (1:200, Abcam), and then incubated with Alexa-Fluor-555-conjugated goat anti-mouse antibody (1:500, Abcam).

Preparation of homogenates, cytosol and microsomes

After CAECs were washed twice with PBS, cells were homogenized in ice-cold HEPES buffer containing 25 mM Na-HEPES, 255 mM sucrose, 1 mM EDTA, and 0.1 mM phenylmethylsulfonyl fluoride (pH 7.4). After centrifugation at 1000 ***g*** for 10 minutes at 4℃, the supernatants containing the membrane protein and cytosolic components, termed homogenates, were frozen in liquid N_2, and stored at −80℃ until use. Microsomal and cytosolic fractions were prepared by a sequential centrifugation of the homogenate at 10,000 ***g*** for 20 minutes and 100,000 ***g*** for 90 minutes, as described previously (Zhang et al., 2001).

RNA interference

siRNAs 5′-GGGAGGAAGCCTAGATGGTC-3′ and 5′-GACTTGCCATCAGTGAACCTCTCTA-3′ were used to silence the genes encoding dysferlin and AHNAK, respectively. These siRNAs were synthesized by Invitrogen according to the bovine gene sequence and were confirmed to efficiently knock down their respective target genes in CAECs in preliminary experiments. The scrambled siRNA (5′-AATTCTCCGAACGTGTCACGT-3′) was also confirmed as a non-silencing double stranded RNA (Zhang, A. Y. et al., 2007) and was used as a control. Transfection of siRNA was performed using the Qiagen TransMessenger transfection kit (Valencia, CA) according to the manufacturer's instructions.

Membrane raft clustering and colocalization studies

Control and FasL-stimulated CAECs were fixed with 4% paraformaldehyde in PBS for 10 minutes. After labeling with Alexa-Fluor-488–CTXB (2 μg/ml, 2 hours, Molecular Probes, Carlsbad, CA), CAECs were incubated with rabbit anti-dysferlin antibody (1:200), rabbit anti-ASMase antibody (1:500, Santa Cruz Biotechnology), or mouse anti-ceramide antibody (1:200, Alexis Biochemicals, San Diego, CA) and then incubated with goat anti-rabbit Alexa-Fluor-555-conjugated secondary antibody (1:500, Abcam) as described previously (Jin et al., 2008a; Yi et al., 2009).

Patches of ganglioside GM1 identified by staining with Alex-Fluor-488–CTXB represented the membrane raft clusters. Clustering of membrane rafts was defined as two or more intense patches of fluorescence on the cell surface, whereas unstimulated cells displayed a homogenous distribution of fluorescence throughout the membrane. In each experiment, the presence or absence of clustering in samples of 200 cells was scored by two independent observers. Images were taken with an Olympus Fluoview confocal microscope, and data were processed with Fluoview W/O3D version 5.0 software. The scan parameters used for all cells were as follows: scan speed, slow; scan model: seq; offset: 1.0 ×. The intensity was 5 and 50 for green and red channels, respectively, and the PMT for green and red channels are 824 and 926, respectively. Colocalization was analyzed by the 'co-localization assay' function in Image Pro Plus software (Version 6.0). The correlation between the green and red color pair was calculated, and the Pearson's correlation coefficient was used to indicate colocalization as reported previously (Zinchuk et al., 2007).

Flow-cytometric analysis

The translocation of dysferlin and ASMase onto the cell membrane was assessed with flow cytometry as described previously (Varsano et al., 1998). CAECs were harvested and washed with PBS, and then blocked with 1% bovine serum albumin (BSA) for 10 minutes at 4℃. After two washes, the pellet was added to 100 ml PBS and incubated with primary antibody against dysferlin (1:200) or ASMase (1:200) followed by incubation with Alexa-Fluor-555-labeled anti-rabbit secondary antibody (Abcam; 1:500). Stained cells were run through a Guava Easycyte Mini Flow Cytometry System (Guava Technologies, Hayward, CA) and analyzed with Guava acquisition and analysis software (Guava Technologies).

Fluorescence measurement

Control and FasL-stimulated CAECs (FasL, 10 ng/ml, 20 minutes) were fixed with 4% paraformaldehyde in PBS for 10 minutes. Cells were then labeled with Alexa-Fluor-488–CTXB (2 μg/ml, 2 hours, Molecular Probes). Cells were incubated with rabbit anti-dysferlin antibody (1:200) or rabbit anti-ASMase antibody (1:500, Santa Cruz Biotechnology), and then incubated with goat anti-rabbit Alexa-Fluor-488-conjugated secondary antibody (1:500, Abcam, San Francisco, CA), as described previously (Jin et al., 2008a; Yi et al., 2009). Pictures were taken with an Olympus fluorescence microscope BX41 (Olympus America, Center Valley, PA). Exposure time was set to 3.5 seconds. Green fluorescence was calculated by using histogram assay function in Photoshop 7.0 software. Fluorescence was normalized to the cell number in each picture.

Immunoblotting and dot blotting

Control and FasL-stimulated CAECs (FasL, 10 ng/ml, 20 minutes) were washed with PBS twice, and then total proteins were prepared for immunoblot assay. For the determine of cellular GM1 content, 5 μl of lysate of equivalent protein content (10 μg) were dot blotted on nitrocellulose membrane, incubated with HRP-conjugated CTXB (500 ng/ml, Sigma) and revealed by chemiluminescence as described previously (Pang et al., 2004).

Flotation of membrane raft fractions

Detergent-resistant membrane fraction flotation was used to evaluate membrane raft clustering in CAECs as we reported previously (Jia et al., 2008). In brief, CAECs were homogenized by five passages through a 25-gauge needle in lysis buffer. Homogenates were layered onto a step gradient consisting of 40%, 30%, and 5% OptiPrep Density Gradient medium, and then the samples were centrifuged at 32,000 r.p.m. for 30 hours at 4℃ using a SW32.1 rotor. Fractions were collected from top to bottom. After addition of an equal volume of 30% trichloroacetic acid, the precipitated proteins were spun down by centrifugation at 13,000 r.p.m. at 4℃ for 15 minutes. The protein pellet was carefully washed with cold acetone and then used for immunoblot analysis.

Assay of ASMase activity

The activity of ASMase was measured as described previously (Yi et al., 2004). Briefly, cell homogenates (20 μg) were incubated with 0.02 μCi of N-methyl-[^{14}C]sphingomyelin in 100 μl acidic reaction buffer containing 100 mM sodium acetate, and 0.1% Triton X-100, pH 5.0 at 37℃ for 15 minutes. The reaction was

terminated with 1.5 ml chloroform:methanol (2:1) and 0.2 ml double-distilled water. After vortexing and centrifuging at 1000 ***g*** for 5 minutes to separate into two phases, the upper aqueous phase containing the *N*-methyl-[^{14}C]sphingomyelin metabolite, [^{14}C]choline phosphate, was measured in a Beckman liquid scintillation counter. The choline phosphate formation rate was calculated to represent the enzyme activity.

FM1-43 quenching

FM1-43 quenching and dequenching experiments were performed to detect lysosomal fusion to the cell membrane of CAECs as we described previously (Bao et al., 2010). For quenching experiments, lysosomes of CAECs were loaded with 8 μM FM1-43 (Molecular Probes) for 2 hours, and then 1 mM BPB was added to the extracellular medium. FM1-43 fluorescence was monitored under confocal microscopy (Olympus) with a low power laser (λ excitation=488 nm). When lysosomes fuse to the cell membrane, BPB enters cells and lysosomes to quench FM1-43 fluorescence (Harata et al., 2006; Zhang, Z. et al., 2007). If there is no lysosome fusion, FM1-43 fluorescence quenching does not occur.

Electron spin resonance spectrometry

Electron spin resonance spectrometry was performed for detection of $O_2\cdot^-$ as we described previously (Zhang, A. Y. et al., 2006). CAECs were gently collected and suspended in modified Krebs-HEPES buffer: 99.01 mM NaCl, 4.69 mM KCl, 1.87 mM $CaCl_2$, 1.20 mM $MgSO_4$, 1.03 mM K_2HPO_4, 25.0 mM $NaHCO_3$, 20.0 mM Na-HEPES and 11.1 mM glucose, pH 7.4), supplemented with deferoxamine (100 μM; metal chelator). Approximately 1×10^6 cells were then incubated with FasL (10 nM) for 15 minutes; these cells were subsequently mixed with 1 mM of the $O_2\cdot^-$-specific spin trap 1-hydroxy-3-methoxycarbonyl-2,2,5,5-tetramethylpyrrolidine (CMH) in the presence or absence of manganese-dependent superoxide dismutase (SOD, 500 U/ml, Sigma). The cell mixture was then loaded into glass capillaries and immediately kinetically analyzed for $O_2\cdot^-$ production for 10 minutes. The SOD-inhibitable fraction of the signal was compared. The ESR settings were as follows: biofield, 3350; field sweep, 60 G; microwave frequency, 9.78 GHz; microwave power, 20 mW; modulation amplitude, 3 G; 4096 points of resolution; receiver gain, 100; and kinetic time, 10 minutes.

Endothelium-dependent vasodilation in isolated small coronary arteries

Fresh bovine hearts were obtained from a local abattoir. Small coronary arteries (~200 μm inner diameter) were dissected and stored in cell culture medium, and then mounted in a Multi Myograph 610M (Danish Myo Technology, Aarhus, Denmark) for recording of their isometric wall tension as described previously (Brandin et al., 2003; Bund and Lee, 2003). After 30 minutes of equilibration in physiological saline solution (PSS, pH 7.4) containing: 119 mM NaCl, 4.7 mM KCl, 1.6 mM $CaCl_2$, 1.17 mM $MgSO_4$, 1.18 mM NaH_2PO_4, 2.24 mM $NaHCO_3$, 0.026 mM EDTA and 5.5 mM glucose at 37℃ bubbled with a gas mixture of 95% O_2, 5% CO_2 to establish the baseline tension, the arteries were then precontracted with a thromboxane A_2 analog, U-46619 (Sigma). Once steady-state contraction was obtained, cumulative dose-response curves to the endothelium-dependent vasodilator, bradykinin (10^{-10} to 10^{-6} M), were determined by measuring changes in wall tension. The ultrasound microbubble technology was used to transfect the endothelium-intact arteries with scrambled siRNA or dysferlin siRNA as we and others described previously (Zhang, F. et al., 2006; Li et al., 2008). Some arteries were treated with the lysosome function inhibitor Baf (100 nM) or the NADPH oxidase inhibitor apocynin (100 μM). Then, the arterial preparations were treated with FasL (10 ng/ml) for 20 minutes, and cumulative dose-response curves to bradykinin were re-recorded.

Synthesis of lipid-binding peptide and its mutant

We performed alignment analysis of the bovine dysferlin sequence with that from zebrafish, mouse and human, a 20 amino acid peptide was designed according to the conserved domain of dysferlin C2A, namely, ELLVVVKDHET-MGRNRFLGE. Also, a 20 amino acid peptide with the V (valine) replaced with D (aspartic acid) was designed to evaluate the effect of dysferlin mutation, namely, ELLDVVKDHETMGRNRFLGE. A third peptide corresponding to the dysferlin C2F domain was designed to evaluate the possible involvement of this C2 domain or as negative control, namely, YIPCTLEPVFGKMFELTC. All these peptides were synthesized by RS Synthesis (Louisville, KY), and the purity of each peptide was above 95% as shown by high-performance liquid chromatography (HPLC) analysis.

Vesicle preparation and lipid-binding assay

To confirm the efficiency of synthetic peptides to bind lipids for competitive assay of lipid of lysosomes, lipid vesicles were prepared by hydration of dried lipid in TE buffer (10 mM Tris-HCl, 1 mM EDTA, pH 7.4), followed by probe sonication until the solution clarified, and samples was centrifuged at 16,000 ***g*** for 5 minutes to remove undissolved debris. All vesicles were used on the day of preparation (Johnson et al., 1998). Peptide stocks and lipid vesicles used in this assay were made in 10 mM HEPES (pH 7.4). 150 μl peptide (40 nM, determined by preliminary experiments that treated cells with 10, 20, 40, 80 and 160 nM) and 150 μL lipid vesicles (1000 nM) were incubated at room temperature for 30 minutes. 200 μL samples were then transferred to a Microcon-100 filtration unit (molecular weight cut-off of 100,000, Invitrogen, CA) and centrifuged with ICE Clinical Centrifuge (set 4) for 5 minutes. Peptide concentration in 100 μl flow-through fraction (unbound peptide) and 100 μl peptide solution (20 nM, 100 μl) before binding experiment was quantified with an o-phthaldialdehyde assay as described previously (Johnson et al., 1998). Briefly, a standard curve was composed of 0, 10, 20, 40, 80 nM of the peptide to be assayed. The samples were used for the measurement on an FLx800 fluorescence microplate spectrophotometer (Bio-Tek Instruments) with excitation at 360/40 nm and emission at 460/40 nm. The peptide-binding capacity was evaluated by comparing the concentrations in the solution before and after binding experiments.

Statistics

Data are presented as means ± s.e.m. Significant differences between and within multiple groups were examined using ANOVA for repeated measures, followed by Duncan's multiple-range test. $P<0.05$ was considered statistically significant.

Funding

This study was supported by grants from the National Institutes of Health [grant numbers HL-57244, HL-75316 and HL-091464]. Deposited in PMC for release after 12 months.

Supplementary material available online at
http://jcs.biologists.org/lookup/suppl/doi:10.1242/jcs.094565/-/DC1

References

Azakir, B. A., Di Fulvio, S., Therrien, C. and Sinnreich, M. (2010). Dysferlin interacts with tubulin and microtubules in mouse skeletal muscle. *PLoS ONE* **5**, e10122.

Bao, J. X., Jin, S., Zhang, F., Wang, Z. C., Li, N. and Li, P. L. (2010). Activation of membrane NADPH oxidase associated with lysosome-targeted acid sphingomyelinase in coronary endothelial cells. *Antioxid. Redox. Signal.* **12**, 703-712.

Bommert, K., Charlton, M. P., DeBello, W. M., Chin, G. J., Betz, H. and Augustine, G. J. (1993). Inhibition of neurotransmitter release by C2-domain peptides implicates synaptotagmin in exocytosis. *Nature* **363**, 163-165.

Brandin, L., Bergstrom, G., Manhem, K. and Gustafsson, H. (2003). Oestrogen modulates vascular adrenergic reactivity of the spontaneously hypertensive rat. *J. Hypertens.* **21**, 1695-1702.

Bund, S. J. and Lee, R. M. (2003). Arterial structural changes in hypertension: a consideration of methodology, terminology and functional consequence. *J. Vasc. Res.* **40**, 547-557.

Cenacchi, G., Fanin, M., De Giorgi, L. B. and Angelini, C. (2005). Ultrastructural changes in dysferlinopathy support defective membrane repair mechanism. *J. Clin. Pathol.* **58**, 190-195.

Chai, Y., Huang, X., Cong, B., Liu, S., Chen, K., Li, G. and Gaisano, H. Y. (2006). Involvement of VAMP-2 in exocytosis of IL-1 beta in turbot (Scophthalmus maximus) leukocytes after Vibrio anguillarum infection. *Biochem. Biophys. Res. Commun.* **342**, 509-513.

Davis, D. B., Doherty, K. R., Delmonte, A. J. and McNally, E. M. (2002). Calcium-sensitive phospholipid binding properties of normal and mutant ferlin C2 domains. *J. Biol. Chem.* **277**, 22883-22888.

Demonbreun, A. R., Fahrenbach, J. P., Deveaux, K., Earley, J. U., Pytel, P. and McNally, E. M. (2011). Impaired muscle growth and response to insulin-like growth factor 1 in dysferlin-mediated muscular dystrophy. *Hum. Mol. Genet.* **20**, 779-789.

Doherty, K. R. and McNally, E. M. (2003). Repairing the tears: dysferlin in muscle membrane repair. *Trends Mol. Med.* **9**, 327-330.

Eum, S. Y., Andras, I., Hennig, B. and Toborek, M. (2009). NADPH oxidase and lipid raft-associated redox signaling are required for PCB153-induced upregulation of cell adhesion molecules in human brain endothelial cells. *Toxicol. Appl. Pharmacol.* **240**, 299-305.

Evesson, F. J., Peat, R. A., Lek, A., Brilot, F., Lo, H. P., Dale, R. C., Parton, R. G., North, K. N. and Cooper, S. T. (2010). Reduced plasma membrane expression of dysferlin mutants is attributed to accelerated endocytosis via a syntaxin-4-associated pathway. *J. Biol. Chem.* **285**, 28529-28539.

Gulbins, E. and Li, P. L. (2006). Physiological and pathophysiological aspects of ceramide. *Am. J. Physiol. Regul. Integr. Comp. Physiol.* **290**, R11-R26.

Han, R., Bansal, D., Miyake, K., Muniz, V. P., Weiss, R. M., McNeil, P. L. and Campbell, K. P. (2007). Dysferlin-mediated membrane repair protects the heart from stress-induced left ventricular injury. *J. Clin. Invest.* **117**, 1805-1813.

Harata, N. C., Choi, S., Pyle, J. L., Aravanis, A. M. and Tsien, R. W. (2006). Frequency-dependent kinetics and prevalence of kiss-and-run and reuse at hippocampal synapses studied with novel quenching methods. *Neuron* **49**, 243-256.

Hochmeister, S., Grundtner, R., Bauer, J., Engelhardt, B., Lyck, R., Gordon, G., Korosec, T., Kutzelnigg, A., Berger, J. J., Bradl, M. et al. (2006). Dysferlin is a new marker for leaky brain blood vessels in multiple sclerosis. *J. Neuropathol. Exp. Neurol.* **65**, 855-865.

Illarioshkin, S. N., Ivanova-Smolenskaya, I. A., Greenberg, C. R., Nylen, E., Sukhorukov, V. S., Poleshchuk, V. V., Markova, E. D. and Wrogemann, K. (2000). Identical dysferlin mutation in limb-girdle muscular dystrophy type 2B and distal myopathy. *Neurology* **55**, 1931-1933.

Jia, S. J., Jin, S., Zhang, F., Yi, F., Dewey, W. L. and Li, P. L. (2008). Formation and function of ceramide-enriched membrane platforms with CD38 during M1-receptor stimulation in bovine coronary arterial myocytes. *Am. J. Physiol. Heart Circ. Physiol.* **295**, H1743-H1752.

Jin, S., Yi, F. and Li, P. L. (2007). Contribution of lysosomal vesicles to the formation of lipid raft redox signaling platforms in endothelial cells. *Antioxid. Redox Signal.* **9**, 1417-1426.

Jin, S., Zhang, Y., Yi, F. and Li, P. L. (2008a). Critical role of lipid raft redox signaling platforms in endostatin-induced coronary endothelial dysfunction. *Arterioscler. Thromb. Vasc. Biol.* **28**, 485-490.

Jin, S., Yi, F., Zhang, F., Poklis, J. L. and Li, P. L. (2008b). Lysosomal targeting and trafficking of acid sphingomyelinase to lipid raft platforms in coronary endothelial cells. *Arterioscler. Thromb. Vasc. Biol.* **28**, 2056-2062.

Johnson, J. E., Rao, N. M., Hui, S. W. and Cornell, R. B. (1998). Conformation and lipid binding properties of four peptides derived from the membrane-binding domain of CTP:phosphocholine cytidylyltransferase. *Biochemistry* **37**, 9509-9519.

Karsan, A., Blonder, J., Law, J., Yaquian, E., Lucas, D. A., Conrads, T. P. and Veenstra, T. (2005). Proteomic analysis of lipid microdomains from lipopolysaccharide-activated human endothelial cells. *J. Proteome Res.* **4**, 349-357.

Kobayashi, T. and Arakawa, Y. (1991). Transport of exogenous fluorescent phosphatidylserine analogue to the Golgi apparatus in cultured fibroblasts. *J. Cell Biol.* **113**, 235-244.

Lek, A., Evesson, F. J., Sutton, R. B., North, K. N. and Cooper, S. T. (2011). Ferlins: regulators of vesicle fusion for auditory neurotransmission, receptor trafficking and membrane repair. *Traffic* **13**, 185-194.

Lennon, N. J., Kho, A., Bacskai, B. J., Perlmutter, S. L., Hyman, B. T. and Brown, R. H., Jr (2003). Dysferlin interacts with annexins A1 and A2 and mediates sarcolemmal wound-healing. *J. Biol. Chem.* **278**, 50466-50473.

Li, N., Yi, F., Sundy, C. M., Chen, L., Hilliker, M. L., Donley, D. K., Muldoon, D. B. and Li, P. L. (2007). Expression and actions of HIF prolyl-4-hydroxylase in the rat kidneys. *Am. J. Physiol. Renal Physiol.* **292**, F207-F216.

Li, N., Chen, L., Yi, F., Xia, M. and Li, P. L. (2008). Salt-sensitive hypertension induced by decoy of transcription factor hypoxia-inducible factor-1alpha in the renal medulla. *Circ. Res.* **102**, 1101-1108.

Li, P. L., Zhang, Y. and Yi, F. (2007). Lipid raft redox signaling platforms in endothelial dysfunction. *Antioxid. Redox Signal.* **9**, 1457-1470.

Matsuda, C., Aoki, M., Hayashi, Y. K., Ho, M. F., Arahata, K. and Brown, R. H., Jr (1999). Dysferlin is a surface membrane-associated protein that is absent in Miyoshi myopathy. *Neurology* **53**, 1119-1122.

McNeil, A. K., Rescher, U., Gerke, V. and McNeil, P. L. (2006). Requirement for annexin A1 in plasma membrane repair. *J. Biol. Chem.* **281**, 35202-35207.

Pang, H., Le, P. U. and Nabi, I. R. (2004). Ganglioside GM1 levels are a determinant of the extent of caveolae/raft-dependent endocytosis of cholera toxin to the Golgi apparatus. *J. Cell Sci.* **117**, 1421-1430.

Reddy, A., Caler, E. V. and Andrews, N. W. (2001). Plasma membrane repair is mediated by Ca(2+)-regulated exocytosis of lysosomes. *Cell* **106**, 157-169.

Shao, D., Segal, A. W. and Dekker, L. V. (2003). Lipid rafts determine efficiency of NADPH oxidase activation in neutrophils. *FEBS Lett.* **550**, 101-106.

Therrien, C., Di Fulvio, S., Pickles, S. and Sinnreich, M. (2009). Characterization of lipid binding specificities of dysferlin C2 domains reveals novel interactions with phosphoinositides. *Biochemistry* **48**, 2377-2384.

Touyz, R. M. (2006). Lipid rafts take center stage in endothelial cell redox signaling by death receptors. *Hypertension* **47**, 16-18.

Uchida, K., Emoto, K., Daleke, D. L., Inoue, K. and Umeda, M. (1998). Induction of apoptosis by phosphatidylserine. *J. Biochem.* **123**, 1073-1078.

Varsano, S., Rashkovsky, L., Shapiro, H. and Radnay, J. (1998). Cytokines modulate expression of cell-membrane complement inhibitory proteins in human lung cancer cell lines. *Am. J. Respir. Cell. Mol. Biol.* **19**, 522-529.

Yi, F., Zhang, A. Y., Janscha, J. L., Li, P. L. and Zou, A. P. (2004). Homocysteine activates NADH/NADPH oxidase through ceramide-stimulated Rac GTPase activity in rat mesangial cells. *Kidney Int.* **66**, 1977-1987.

Yi, F., Jin, S., Zhang, F., Xia, M., Bao, J. X., Hu, J., Poklis, J. L. and Li, P. L. (2009). Formation of lipid raft redox signalling platforms in glomerular endothelial cells: an early event of homocysteine-induced glomerular injury. *J. Cell Mol. Med.* **13**, 3303-3314.

Zhang, A. Y., Yi, F., Zhang, G., Gulbins, E. and Li, P. L. (2006). Lipid raft clustering and redox signaling platform formation in coronary arterial endothelial cells. *Hypertension* **47**, 74-80.

Zhang, A. Y., Yi, F., Jin, S., Xia, M., Chen, Q. Z., Gulbins, E. and Li, P. L. (2007). Acid sphingomyelinase and its redox amplification in formation of lipid raft redox signaling platforms in endothelial cells. *Antioxid. Redox Signal.* **9**, 817-828.

Zhang, D. X., Fryer, R. M., Hsu, A. K., Zou, A. P., Gross, G. J., Campbell, W. B. and Li, P. L. (2001). Production and metabolism of ceramide in normal and ischemic-reperfused myocardium of rats. *Basic Res. Cardiol.* **96**, 267-274.

Zhang, F., Zhang, G., Zhang, A. Y., Koeberl, M. J., Wallander, E. and Li, P. L. (2006). Production of NAADP and its role in Ca2+ mobilization associated with lysosomes in coronary arterial myocytes. *Am. J. Physiol. Heart Circ. Physiol.* **291**, H274-H282.

Zhang, Z., Chen, G., Zhou, W., Song, A., Xu, T., Luo, Q., Wang, W., Gu, X. S. and Duan, S. (2007). Regulated ATP release from astrocytes through lysosome exocytosis. *Nat. Cell Biol.* **9**, 945-953.

Zinchuk, V., Zinchuk, O. and Okada, T. (2007). Quantitative colocalization analysis of multicolor confocal immunofluorescence microscopy images: pushing pixels to explore biological phenomena. *Acta Histochem. Cytochem.* **40**, 101-111.